Latent tracks in sapphire induced by 20-MeV fullerene beams

S. M. M. Ramos, N. Bonardi, and B. Canut
Département de Physique des Matériaux (UMR CNRS 5586), Université Claude Bernard Lyon I, 69622 Villeurbanne Cedex, France

S. Della-Negra
Institut de Physique Nucléaire, CNRS-IN2P3, 91406 Orsay, France

(Received 27 May 1997)

Single crystals of α-Al_2O_3 were irradiated with 20-MeV fullerene beams in a fluence range from 1.0×10^{10} to 2.2×10^{11} $C_{60}^{+}\,cm^{-2}$. The cluster electronic stopping power $(dE/dx)_e$ was approximately 62 keV nm^{-1}. Two complementary techniques were employed to assess the modifications induced by these irradiations: Rutherford-backscattering spectrometry in channeling geometry (RBS-C) and transmission electron microscopy (TEM). The disorder induced by electronic processes is clearly determined by the RBS-C analysis. A damage cross section A_e of about 2.2×10^{-12} cm^2 has been extracted from the disorder kinetics, which corresponds to a track radius of $\approx$8.5 nm. From lattice-disorder profiling, a maximal decorrelation length of the C_{60} clusters in the crystal was estimated to be $\approx$150 nm. TEM micrographs exhibit cylindrical latent tracks formed around the projectile trajectory, while the high-resolution observations evidence the amorphization of sapphire in the core of these tracks. The present results have been interpretated within a model of high locally deposited energy densities in the cluster irradiation regime. [S0163-1829(98)01701-9]

I. INTRODUCTION

It is now well established that the electronic stopping power $(dE/dx)_e$ of fast heavy ions can induce stable defects in a large variety of radiolysis resistant insulators. Several studies of the damage morphology induced by high electronic deposition in refractory oxides are at present found in the literature.[1–8] In particular, in the last few years we have investigated the damage induced by GeV ion irradiations in two oxides: lithium niobate ($LiNbO_3$) and sapphire (α-Al_2O_3).[4–7] Our previous results show that in $LiNbO_3$ single crystals extended defects are created above a $(dE/dx)_e$ of 6.0 keV nm^{-1}, while the amorphization occurs above 10 keV nm^{-1} with latent track formation. However, the same effects were not observed in sapphire. In such an oxide, for $(dE/dx)_e$ values up to 42.7 keV nm^{-1} (maximum value reached in this material with ^{238}U ions of 2.8 MeV/u incident energy), neither amorphization nor latent track formation were found. However, extended defects are detected above 20 keV nm^{-1}. The only route to overcome the GANIL monoatomic beam limitation is to use energetic clusters (C_{60}) as incident projectiles. For such irradiation conditions, taking into account the additivity rule of the individual stopping powers recently evidenced by Baudin *et al.*,[9] a higher $(dE/dx)_e$ can be reached. For example, a value of 62.4 keV nm^{-1} may be obtained with 20-MeV C_{60} clusters in α-Al_2O_3. In addition, the very low velocity of these clusters compared to GANIL ions, enhances the deposited electronic energy density. This confinement effect can lead to drastic structural modifications as reported by Dammak *et al.*[10] for metallic targets bombarded with MeV C_{60} clusters.

In this work we investigate the damage induced in α-Al_2O_3 single crystals by fullerene irradiations in the MeV energy range. One question is open: Is it possible to amorphize sapphire targets by such huge electronic excitations? In order to answer this question, the damage morphology has been characterized by Rutherford-backscattering spectrometry in channeling geometry (RBS-C) analysis and transmission electron microscopy (TEM) observations.

II. EXPERIMENTAL PROCEDURE

High purity α-Al_2O_3 single crystals having an $\langle0001\rangle$ axis oriented normal to the surface were optically polished and annealed for 120 h at 1723 K to remove the residual polishing surface damage. The minimum yield $\chi_v=2.5\%$ measured at the low-energy side of the aluminum surface peak in the RBS-C spectrum of a pristine sample indicates that this thermal treatment was quite satisfactory. The samples were then irradiated at room temperature with a 20-MeV C_{60}^{+} cluster beam provided by the tandem accelerator at Institut de Physique Nucleaire d'Orsay. The fluences ranged from 1.0×10^{10} to 2.2×10^{11} $C_{60}^{+}\,cm^{-2}$ and the flux was about 1.3×10^{7} cluster $cm^{-2}\,s^{-1}$ on a 7-mm^2 irradiated surface. The main irradiation parameters, deduced from TRIM code[11] in conjunction with the relative velocities $\beta=v/c$ (where v is the velocity of the ions and c is the light velocity) are listed in Table I. In these calculations, performed with 333-keV monoatomic carbon, it has been assumed that the incident energy loss of the projectile is the sum of the energy losses of the individual carbon ions. In order to check the possible contribution of elastic displacements induced per incident cluster to the damage created at the sample surface, the theoretical nuclear damage cross section A_n has been added in Table I. It has been calculated assuming a displacement energy of 75 and 16 eV per oxygen and aluminum atoms, respectively.[12]

RBS-C analyses were performed using a beam of 2.0 MeV He^{+} at near-normal incidence to the sample surface and scattered into a surface-barrier detector set at 150°. Ion channeling measurements were made with the beam aligned along the $\langle0001\rangle$ axis. In order to minimize the charge build

TABLE I. Main features of the cluster irradiations in α-Al_2O_3 single crystals: incident energy (E), incident electronic $[(dE/dx)_e]$ and nuclear $[(dE/dx)_n]$ stopping powers, projected range (R_p), relative velocity ($\beta = v/c$) and the maximum energy ($E_m = 2\ mv^2$) transferred to δ electrons. In the last column A_n is the theoretical nuclear damage cross section.

Projectile	E (MeV)	$(dE/dx)_e$ (keV nm^{-1})	$(dE/dx)_n$ (keV nm^{-1})	R_p (nm)	$\beta = v/c$ (%)	E_m (eV)	A_n ($\times 10^{-15}$ cm^2)
C_{60}	20	62.4	2.1	428	0.77	59.8	3.8

up at the surface of these insulating crystals during backscattering analysis, the beam current was limited to around 10 nA and the irradiated surface area of samples never exceeded 1 mm^2.

Before irradiation some of α-Al_2O_3 single crystals were preliminary prepared for TEM observations in plane view configuration. These specimens were mechanically thinned down to about 50 μm and then ion milled using 5 keV argon bombardment of 1.0 mA and a milling angle of 15°. The samples were then irradiated at a fixed fluence of 1.0×10^{10} C_{60}^+ cm^{-2} and the observations were performed using TOP CON 002B equipment, operating at 200 KV and offering a resolution of 0.18 nm.

III. RESULTS AND DISCUSSION

Typical RBS-C results are shown in Fig. 1 which presents random (a) and aligned (b) spectra obtained in α-Al_2O_3 irradiated with a fluence of 2.2×10^{11} C_{60}^+ cm^{-2}. For comparison the aligned spectrum of the pristine crystal is also presented (c). Whatever the energy, curve (b) lies distinctly above curve (c). This is evidently related to the damage created in both oxygen and aluminum sublattices. However, due to the poor RBS sensitivity for detecting low atomic masses such as oxygen, the disorder calculations have been carried out only from the aluminum signal by first measuring the dechanneling yield χ at the low-energy edge of the aluminum surface peak. By taking into account the minimum yield corresponding to the pristine crystal χ_v the relative disorder α at the sapphire surface will be given by

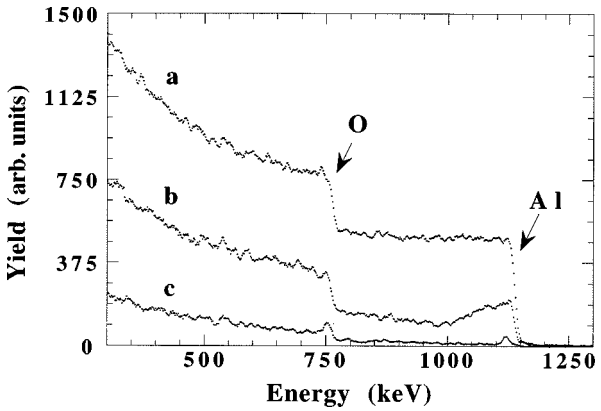

FIG. 1. RBS-C spectra for α-Al_2O_3 single crystal irradiated with 2.2×10^{11} C_{60}^+ cm^{-2} at 20 MeV incident energy (a) and (b) random and channeled spectra, respectively; (c) channeled spectrum of a virgin sample. Analysis conditions: 2 MeV $^4He^+$ beam; detection angle 150°.

$$\alpha = \frac{\chi - \chi_v}{1 - \chi_v}. \tag{1}$$

From the fluence evolution of the disorder ratio, a damage cross section A_e was determined using the Poisson's law. This kinetic is based on a direct impact model and assumes a saturation value of 100% for disorder:[13]

$$\alpha = 1 - \exp(-\phi A_e), \tag{2}$$

where ϕ is the irradiated fluence. The value obtained for A_e in our experiments is 2.2×10^{-12} cm^2, which is almost two orders of magnitude higher than the nuclear contribution A_n for defect creation (Table I). So, the disorder measured by RBS-C experiments is necessarily due to the high rate of electronic energy deposited by the clusters in the near surface target. From a comparison between the present results and those previously obtained with swift heavy ions at GANIL two main features can be pointed out.

(i) An extrapolation of GANIL results on sapphire to a same $(dE/dx)_e$ range obtained with the cluster beam, gives $A_e \approx 3.5 \times 10^{-13}$ cm^2, which is at least six times lower than the A_e value obtained in this study. The higher efficiency of cluster beams to create damage via electronic processes is clearly confirmed in our targets. This effect has been ascribed to the very low values of relative velocities ($\beta < 1\%$) of C_{60}^+ projectiles which limit both the maximum kinetic energy E_m and the maximum radial range ($r_\delta < 1$ nm) of δ electrons emitted during the ionization process (Table I). In these conditions, the deposited energy density (W) is highly confined around the projectile trajectory and it reaches much larger values ($W \approx$ hundred eV/atom) than those obtained with GANIL irradiations by monoatomic beam in the same range of $(dE/dx)_e$.

(ii) Previous studies performed with GeV ions in refractory oxides of different ionicities such as $LiNbO_3$ and α-Al_2O_3 have shown that for similar values of $(dE/dx)_e$ and velocities, the damage cross section varies conversely with the oxide ionicity [e.g., $A_e = 1.3 \times 10^{-13}$ cm^2 in sapphire[4] and $A_e = 1.2 \times 10^{-12}$ cm^2 in $LiNbO_3$ (Ref. 14)]. Note that the same hierarchy in the damage sensitivity is also systematically observed in the elastic collisions regime.[15–18] This difference between the A_e values in the GANIL regime is strongly reduced for the fullerene irradiation conditions. Recently Bonardi *et al.*[19] measured a damage cross section of 3.4×10^{-12} cm^2, in $LiNbO_3$ under 30 MeV C_{60}^+ irradiations $[(dE/dx)_e \approx 65$ keV nm$^{-1}]$. This value is only 50% higher than the above mentioned damage cross section in sapphire. Such nearly equal damage cross section values suggest that the role played in the damage process by the physicochemi-

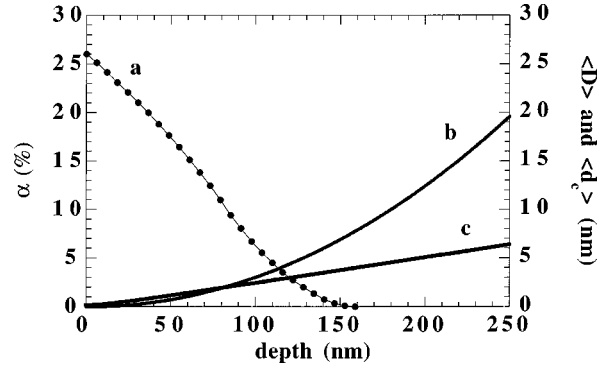

FIG. 2. Relative disorder α determined from the RBS-C spectrum given in Fig. 1 [curve (a)], the average distance between two carbons in the cluster [curve (b)] and the Coulomb repulsion between two carbon ions at the equilibrium charge state [curve (c)].

cal properties of each of these oxides is minimized when the irradiation conditions induce the drastic structural changes.

Another striking feature observed on the spectrum (b) in Fig. 1 is the quick decrease of the relative disorder which, in agreement with previous studies,[20] can be attributed mainly to the scattering of the individual carbon atoms after the cluster fragmentation on the target surface. The damage depth profile determined by using a method described elsewhere,[21] is displayed in Fig. 2. From the experimental profile the depth at which the initial disorder drops to zero is $\approx$150 nm. Taking into account both the TRIM calculations[11] and the additivity of the individual stopping powers of carbon ions, the electronic stopping power of the C_n projectiles at this depth is approximately 44 keV nm^{-1} for $n=60$ (Fig. 3). This value is significantly higher than the threshold in electronic energy loss ($\approx$20 keV nm^{-1}) for defect (point or extended) creation in this oxide. The absence of any significant disorder beyond the referred depth indicates that the cluster projectile has lost about 50% of its components along its path [e.g., for $n=30$, the cluster $(dE/dx)_e$ would be $\approx$22 keV nm^{-1}]. Consequently, the damage layer thickness may be regarded as a reasonable estimate for the maximal decorrelation length L_M, of the incident clusters. In order to compare the experimental profile with theoretical predictions, we have calculated the average distance between two neighbor carbon atoms as a function of the depth. Two different processes contribute to increase the distance between the cluster components along the projectile path: (i) the angular straggling, due to nuclear collisions at small impact parameter between carbon and host atoms. (ii) The Coulomb repulsion between the individual carbon ions, due to their effective charge at equilibrium charge state. The following procedure was adopted to take into account these effects.

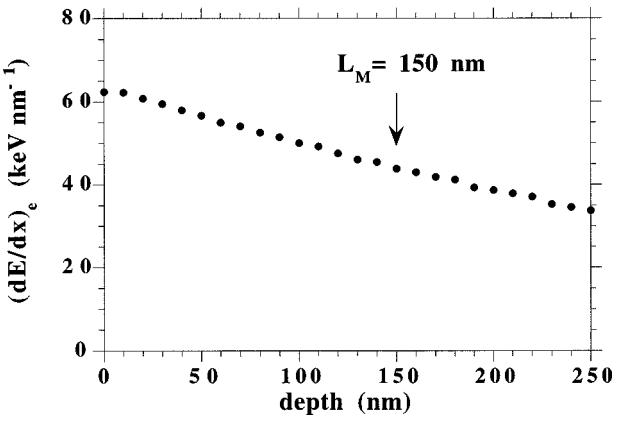

FIG. 3. Electronic stopping power evolution with depth.

(i) By simulating (with the TRIM code) a carbon implantation into sapphire at 333 keV incident energy, we have calculated the depth dependence of the transverse straggling (ΔR_t) characteristic of the incident particles scattering assuming a Gaussian radial distribution.

(ii) We have assumed that the sixty carbon atoms from fullerene are evenly distributed in a circular area of a $2\Delta R_t$ radius.

(iii) The mean distance between two carbon atoms in this area is then calculated from

$$\langle D\rangle = \sqrt{\frac{\pi(2\Delta R_t)^2}{60}}. \tag{3}$$

(iv) In order to evaluate the Coulomb repulsion contribution we have calculated as function of the depth the internuclear distance $\langle d_c\rangle$ between two carbon atoms[22] from the following expression:

$$\langle d_c\rangle = \sqrt{\frac{4\pi r^2}{60}}. \tag{4}$$

In our calculations we have assumed that the cluster components are evenly distributed on a homogeneous charged spherical surface having an initial radius r_0 equal to the radius of a free C_{60} cluster ($r_0=0.35$ nm). Assuming also that the effective charge of the ions (calculated at the incident energy) remains constant,[23,24] we have calculated as a function of the depth the radius r of the spherical charge distribution. These values were inserted in relation (4) to determine $\langle d_c\rangle$. The results of these calculations are presented in curve (b) and (c) of Fig. 2. A correlation between the depth profile and the depth evolution of both $\langle D\rangle$ and $\langle d_c\rangle$ is clearly observed. In the first $\approx$60 nm, where the average distance between two carbon atoms is maximally $\approx$1.0 nm, these two contributions are of the same order of magnitude. However, the balance between the two contributions is modified at larger depth values. At a depth of $\approx$150 nm, where the relative disorder vanishes, the projectile scattering process necessary to separate the cluster fragments is about twice the Coulomb repulsion contribution, i.e., in agreement with previous studies performed with small clusters (C_n, $n=2$, 4, 6, and 8) in $LiNbO_3$.[20] Note that at this depth the mean distance between two carbon atoms deduced from curve (b) is $\approx$7.0 nm. This value exceeds the radial range of δ electrons ($<$1.0 nm) by one order of magnitude. In order to relate the mean distance between two clusters components at given a depth and the corresponding lattice disorder, theoretical calculations based on a probabilistic approach are presently carried out.

Electron microscopy observations were performed on a prethinned sapphire irradiated with 1.0×10^{10} C_{60}^+ cm^{-2}. TEM micrographs displayed in Fig. 4 show a distribution of spherical defects. The surface density of these defects is in agreement with the irradiation fluence, indicating that each

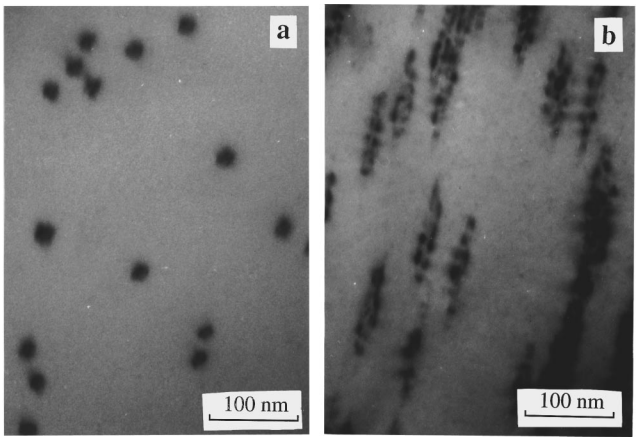

FIG. 4. Plane view micrographs of sapphire irradiated with 1.0×10^{10} C_{60}^{+} cm^{-2}. The images were taken in two different configurations: (a) with the electron direction parallel to the ion beam; (b) with the sample tilted 42° in the microscope.

defect corresponds to one projectile impact. By tilting the sample during the observations, cylindrical tracks extending along the projectile paths are clearly visualized [Fig. 4(b)]. Assuming that the sample thickness is sufficient to include the entire track, a track length of 145 ± 15 nm was determined from twenty individual track measurements. This value, in good agreement with the decorrelation length determined in Fig. 2 from RBS-C results, gives a reasonable estimate of the spatial correlation of the cluster projectile during the slowing down process in the solid. From a TEM picture [Fig. 5(a)] obtained at higher magnification, a radius of 5.5 ± 1.0 nm was directly measured. This value is nearly one time and half smaller than the track radius deduced from damage cross section measurements ($A_d = \pi r^2$, $r \approx 8.5$ nm) by RBS-C analysis. This difference can be understood considering that the radius determined by TEM images concerns only the core tracks, while the disorder measured by RBS-C takes into account both the core track and the shell of stressed material surrounding the core. In order to get more information on these defects, high-resolution electron microscopy (HREM) was used. In the HREM image [Fig. 5(b)] the contrast of the bright zone reveals the amorphization of sapphire inside the latent tracks. This amorphization has been confirmed by a numerical Fourier transform of the direct image. At the start of our observations, a quick decrease of the amorphous radius with time is detected, indicating that a solid phase epitaxy induced by the electron beam occurs. However, after approximately five minutes the movement of the atomic planes is reduced and the images become stable as shown in Fig. 5(b). In this picture the amorphous zone is partially restored and an amorphous core radius of ≈ 3.3 nm is observed. It is surrounded by a darker contrast probably due to the strain around the amorphous region. The high resistance of sapphire to amorphization and a mean distance between two tracks close to 100 nm might also contribute to the metastability of the amorphous phase. A detailed study of the amorphous phase stability in sapphire is now underway, using fullerene beams of higher energy.

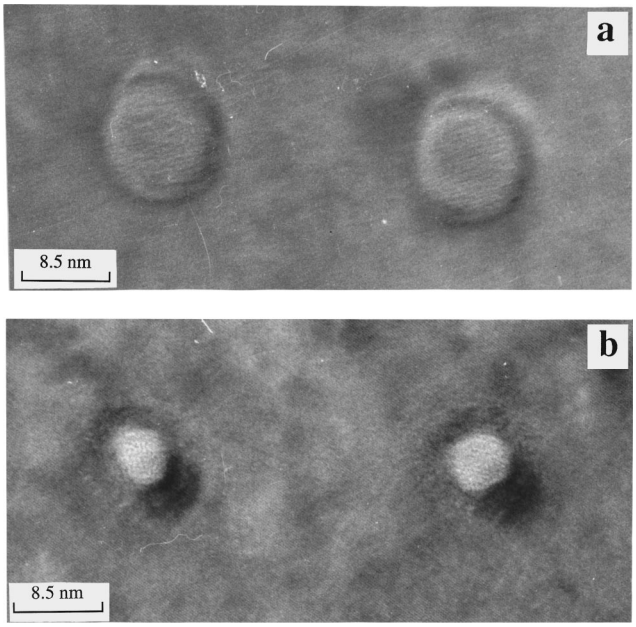

FIG. 5. Same sample as in Fig. 4. (a) TEM observation of the track cross sections. (b) HREM images of the latent tracks. The difference between the amorphous region and the crystalline area is clearly evidenced.

Another striking feature deduced from the TEM observations concerns the threshold in electronic energy loss for latent track formation in α-Al_2O_3. The present results show that in the low velocity regime ($\beta \approx 1\%$) this threshold is below 63 keV nm^{-1}. It is worth noticing that in the medium velocity regime ($\beta \approx 10\%$), previously investigated at GANIL, no latent tracks were observed in sapphire up to $(dE/dx)_e \approx 43$ keV nm^{-1}.

IV. CONCLUSION

In this work we have investigated the fullerene irradiation effects in sapphire. Our results exhibit two main features.

(i) The significant disorder measured at the crystal surface by RBS-C analysis implies a damage cross section of 2.2×10^{-12} cm^2, which exceeds at a given $(dE/dx)_e$ the A_e values for monoatomic beams. This difference has been attributed to the higher density of deposited energy in the cluster regime. From the lattice disorder evolution versus depth, a maximal decorrelation length $L_M \approx 150$ nm of the C_{60} clusters was estimated. At larger depth the cluster fragments do not interact and no significant disorder can thus be created.

(ii) For the first time, to our knowledge, the amorphization of sapphire by electronic collective excitations is evidenced. This effect is ascribable to the very high energy density deposited in the tracks. It results from the confinement of all carbon atoms of the cluster which propagate in the same track in a region close to the sample surface.

[1] M. Toulemonde, G. Fuchs, N. Nguyen, F. Studer, and D. Groult, Phys. Rev. B **35**, 6560 (1987).
[2] M. Toulemonde and F. Studer, Philos. Mag. A **58**, 799 (1988).
[3] A. Meftah, F. Brisard, J. M. Constantini, E. Dooryhee, M. Hage-Ali, M. Y. Hervieu, J. P. Stoquer, F. Studer, and M. Toulemonde, Phys. Rev. B **49**, 12 457 (1994).
[4] B. Canut, A. Benyagoub, G. Marest, A. Meftha, N. Moncoffre, S. M. M. Ramos, F. Studer, P. Thevenard, and M. Toulemonde, Phys. Rev. B **51**, 12 194 (1995).
[5] B. Canut, R. Brenier, A. Meftah, P. Moretti, S. Ould Salem, S. M. M. Ramos, P. Thevenard, and M. Toulemonde, Nucl. Instrum. Methods Phys. Res. B **91**, 312 (1994).
[6] S. M. M. Ramos, R. Brenier, B. Canut, G. Fuchs, P. Thevenard, M. Treilleux, A. Meftah, and M. Toulemonde, J. Appl. Phys. **77**, 2952 (1995).
[7] S. M. M. Ramos, B. Canut, M. Ambri, C. Clement, E. Dooryhee, M. Pitaval, P. Thevenard, and M. Toulemonde, Nucl. Instrum. Methods Phys. Res. B **107**, 254 (1996).
[8] M. Beranger, P. Thevenard, R. Brenier, B. Canut, S. M. M. Ramos, A. Brunelle, S. Della-Negra, Y. Le Beyec, E. Balanzat, and T. Tombrello, Phys. Rev. B **53**, 14 773 (1996).
[9] K. Baudin, A. Brunelle, M. Chabot, S. Della Negra, J. Depauw, D. Gardes, P. Hakansson, Y. Le Beyec, A. Billebaud, M. Fallavier, J. Remillieux, J. C. Poizat, and J. P. Thomas, Nucl. Instrum. Methods Phys. Res. B **94**, 341 (1994).
[10] H. Dammak, A. Dunlop, and D. Lesueur, Phys. Rev. Lett. **74**, 1135 (1994).
[11] J. P. Biersack and L. G. Haggmark, Nucl. Instrum. Methods Phys. Res. **174**, 257 (1980).
[12] D. M. Parkin and C. A. Coulter, J. Nucl. Mater. **101**, 261 (1981).
[13] J. F. Gibbons, Proc. IEEE **60**, 1062 (1972).
[14] B. Canut, R. Brenier, A. Meftah, P. Moretti, S. Ould Salem, M. Pitaval, S. M. M. Ramos, P. Thevenard, M. Toulemonde, Radiat. Eff. Defects Solids **136**, 307 (1995).
[15] C. J. McHargue, G. C. Farlow, G. M. Begun, J. M. Williams, C. W. White, B. R. Appleton, P. S. Sklad, and P. Angelini, Nucl. Instrum. Methods Phys. Res. B **16**, 212 (1986).
[16] C. J. McHargue, P. S. Sklad, and C. W. White, Nucl. Instrum. Methods Phys. Res. B **46**, 79 (1990).
[17] S. M. M. Ramos, B. Canut, L. Gea, L. Romana, J. Lebrusq, P. Thevenard, and M. Brunel, Nucl. Instrum. Methods Phys. Res. B **59/60**, 1211 (1991).
[18] P. Moretti, B. Canut, S. M. M. Ramos, P. Thevenard, D. Poker, J. B. M. Da Cunha, L. Amaral, and A. Vasquez, J. Mater. Res. **8**, 2679 (1993).
[19] N. Bonardi, B. Canut, O. Marty, S. M. M. Ramos, and S. Della-Negra (unpublished).
[20] B. Canut, S. Ramos, N. Bonardi, J. Chaumont, H. Bernas, and E. Cottereau, Nucl. Instrum. Methods Phys. Res. B **122**, 335 (1997).
[21] B. Canut, L. Romana, P. Thevenard, and N. Moncoffre, Nucl. Instrum. Methods Phys. Res. B **46**, 128 (1990).
[22] W. Brandt, A. Ratkowski, and R. H. Ritchie, Phys. Rev. Lett. **33**, 1325 (1974).
[23] K. Raghavachari and J. S. Binkley, J. Chem. Phys. **87**, 2191 (1987).
[24] H. Barkas, *Nuclear Research Emulsions* (Academic Press, New York, 1963), Vol. 1, Chap. 9.